Available online at www.sciencedirect.com
ScienceDirect
Acta Biomaterialia 2 (2006) 483–492
Acta BIOMATERIALIA
www.actamat-journals.com

# Role of cell location and morphology in the mechanical environment around meniscal cells

Tumul Gupta, Tammy L. Haut Donahue *

*Department of Mechanical Engineering – Engineering Mechanics, Michigan Technological University, 815 R.L. Smith Building, 1400 Townsend Dr., Houghton, MI 49931, United States*

Received 21 December 2005; received in revised form 23 April 2006; accepted 23 May 2006

**Abstract**

Fibrochondrocytes within meniscal tissue have been shown to alter their biochemical activity in response to changes in their mechanical environment. Meniscal tissue is known to contain both spherical (chondrocytic-like) and elliptical (fibroblastic-like) cells. We hypothesize that a cell's mechanical environment is governed by local material properties of the tissue around the cell, the cell morphology and the cell's position within the tissue. A two-dimensional, non-linear, fiber (collagen) reinforced, multi-scale, finite element model was utilized to quantify changes in the stress, strain, fluid velocity and fluid flow induced shear stress (FFISS) within and around fibrochondrocytes. Cells differing in morphology and size were modeled at different locations within an explant 6 mm in diameter and 5 mm thick, under 5% unconfined compression. Cellular stresses were an order of magnitude less than surrounding extracellular matrix stresses but cellular strains were higher. Cell size affected both the stress and strain levels within the cell, with smaller cells being exposed to smaller principal stresses and strains than larger cells of the same shape. The pericellular matrix of an elliptical cell was less effective at shielding the cell from large principal strains and stresses. FFISS were largest around small circular cells (~0.13 Pa), and were dramatically affected by the position of the cell relative to the axis of the explant, with cells closer to the periphery experiencing greater FFISS than cells near the central axis of the explant. These results will allow biosynthetic activity of fibrochondrocytes to be correlated with position and morphology in the future.


*Keywords:* Meniscus; Material properties; Fibrochondrocyte; FEM; Knee

## 1. Introduction

Menisci within the knee are crucial to its proper function. The triangular cross section of meniscal tissue cradles the articulating surface of the femur allowing the meniscus to carry 50–70% of the static compressive load transmitted through the knee [1,2], with the remaining portion being carried by the underlying articular cartilage. The menisci also assist in shock absorption [3]. The geometry of the meniscus is crucial to its role in transmitting loads through the knee [4] and meniscectomies have been shown to increase contact pressures on the underlying cartilage which leads to osteoarthritis [5–7].

The meniscus is a biphasic tissue composed of both a fluid and solid matrix, with the solid matrix made primarily of proteoglycans and collagen. The compressive strength of meniscal tissue is derived from the interaction of interstitial fluid and proteoglycans whereas the tensile strength is predominantly provided by type I collagen arranged circumferentially [8,9]. The porous nature of the matrix allows for fluid motion under applied physiological loading [8]. It is thought that fibrochondrocytes within meniscal tissue regulate their surroundings according to their mechanical environment, thereby making the meniscus a mechanically sensitive tissue [10,11]. Although static compression degrades meniscal tissue, dynamic loading has been shown to upregulate gene expression for matrix proteins [12].

* Corresponding author. Tel.: +1 906 487 2078; fax: +1 906 487 2822.
*E-mail address:* thdonahu@mtu.edu (T.L. Haut Donahue).

1742-7061/$ - see front matter 
doi:10.1016/j.actbio.2006.05.009

Articular cartilage and meniscus behave in a similar manner, as both are fiber reinforced, biphasic materials. Finite element modeling of the human knee joint under compressive loading of two times body weight indicates that physiological loading of a healthy intact medial meniscus results in approximately 2–10% compressive strains [7]. The response of cartilage explants begins to diverge from a statically loaded case when compression frequencies rise above 0.001 Hz [13,14]. At frequencies above 0.1 Hz an inhomogeneous distribution of biosynthetic activity, measured as proline and sulfate incorporation to indicate aggrecan synthesis and amino acid incorporation, occurs within cylindrical explants. Radial regions of an explant upregulate biosynthetic activity whereas the central regions behave as if statically compressed [13–15]. The biosynthetic profile follows the radial changes in fluid velocity and streaming potentials [15].

Fibrochondrocytes have been shown to change from an elliptical or fibroblastic morphology within superficial regions to a more spherical or chondrocytic morphology in deeper regions [16]. Although the cell has a modulus of elasticity that is lower than that of the extracellular matrix (ECM), the modulus of the pericellular matrix (PCM) lies between that of the cell and the ECM, reducing the disparity between the strains and stresses within the ECM and cell [17]. Following 5% unconfined compressive strain of a cylindrical explant of cartilage, cells populating areas closer to a free edge, and hence experiencing greater fluid motion, underwent larger deformations compared to cells within central regions [18].

Finite element (FE) modeling has been used to study the mechanical environment within musculoskeletal tissues. A previous FE model has shown how differences between matrix properties and cell properties affect the mechanical environment around the cell [17]. Additionally, position within the tissue [18] and cell morphology [19] have previously been studied for their effects on the mechanical environment of chondrocytes. However, how these factors, as they pertain to meniscal tissue, combine to alter or affect the mechanical environment of meniscal cells has yet to be determined. Previous studies of articular cartilage and meniscus suggest that fluid flow induced shear stress (FFISS) is a potent mechanical stimulus eliciting a significant upregulation of intracellular calcium following the onset of fluid flow [20–23]. The magnitude of *in vivo* FFISS in meniscus is presently unknown. Additionally, previous FE models have not included a cell membrane with distinct properties. Although the cell membrane may not be rigid enough to contribute to the structure of the cell, its relatively low permeability may significantly affect the fluid flow patterns and pressure in and around the cell.

We hypothesize that cells at different locations within a meniscal explant are exposed to different magnitudes of stress, strain, fluid flow velocities and associated fluid flow induced shear stresses. We also hypothesize that the elliptical morphology of some fibroblastic-like meniscal cells alters the magnitude of mechanical stimulation of the cell when compared to chondrocytic-like meniscal cells. A non-linear, fiber reinforced, biphasic model of a meniscal explant containing a cellular unit consisting of the cell, its membrane, surrounded by a PCM and a portion of the ECM was utilized in this study to test our hypotheses.

## 2. Methods

A multi-scale modeling approach was utilized to determine the mechanical environment around individual fibrochondrocytes. A cell and the explant were modeled separately as the size of the cell was three orders of magnitude smaller than that of the explant. In order to complement current experimental work, full thickness explants were modeled in two dimensions being 5 mm thick and 6 mm in diameter. This represents the thickest explant that can be harvested from porcine menisci with parallel flat faces. Since the model is homogeneous, the thickness of the explant is relatively insignificant. Only half of the explant was modeled due to symmetry. A submodeling function (ABAQUS, ABAQUS, Inc., Providence, RI) was utilized. This analysis was activated using the *SUBMODEL command which can accommodate a submodel with different element types between the global model and the submodel. The submodeling routine uses the output of the explant model as boundary conditions for the cell model allowing the cell to be modeled as if it were within the explant without requiring an excessive range of element sizes within one single model.

### 2.1. Explant model

Biphasic porous elastic models have been used successfully to model both articular cartilage and meniscus, which have similar microstructure [24–27]. A biphasic model is well accepted to represent the solid matrix and interstitial fluid known to be present in meniscal tissue [8]. The current model is biphasic porous elastic and models interstitial fluid as inviscid water. The specific weight of the interstitial fluid was 9.8 $kN/m^3$. Four-noded, reduced integration plane strain continuum elements (CPE4RP) with pore pressure activated were used for the ECM. Spring elements (collagen fibers) active in tension only were oriented horizontally between the nodes of the homogenous, isotropic continuum elements to simulate tension compression non-linearity (Table 1) [25–29]. Axial spring elements between two nodes (SPRINGA) were used to model collagen. To properly represent the orientation of collagen fibers within the explant, it was necessary to utilize a two-dimensional (2D) model versus an axisymmetric model. While the 2D model presents limitations in not representing the three-dimensional (3D) cellular shape, it allows for a parametric analysis of cell morphology. The 3D shape of meniscal cells is currently unknown and thus, in the future it will be necessary to characterize this for inclusion in a 3D model. Material properties were taken

Table 1
Material properties of meniscal tissue used in the explant global model and their ranges as given in the literature

| Property | Range | Ref. value |
|---|---|---|
| Poisson's ratio of the matrix [30–32] | 0–0.4 | 0 |
| Modulus of elasticity of the matrix MPa (compression) [30–32] | 0.3–0.6 | 0.4 |
| Permeability of the matrix ($10^{-15}$ $m^4$/N s) [30–33] | 0.6–1.5 | 1.5 |
| Spring constant of collagen (N/mm) (tension) [29,34] | 50–200 | 150 |

from previous experimental studies of bovine, canine, human and porcine meniscus. Variations in the species, age and measurement techniques used by these researchers produced the range of values for each variable (reference values are shown in Table 1) [29–34]. Each element was 0.025 mm × 0.025 mm. Coupled pore fluid diffusion and stress analysis (ABAQUS Analysis User's Manual 6.7) was used to analyze the fluid flow velocities, pore pressures, stresses and strains within the explant. Transient analysis was invoked to include time dependent effects such as the viscoelastic effect of fluid flow through the permeable matrix. Fluid velocities and pore pressures were calculated at the integration points and corner nodes of each element, respectively.

### 2.1.1. Boundary conditions

Five percent strain, unconfined ramp compression was applied linearly to the superficial surface of the explant model over 1 s, as this has previously been shown to be within the normal physiological range of 2–10% strain [7]. Unconfined compression was simulated at the unconstrained right most edge of the 2D model (free edge of the explant) by specifying a zero pore pressure boundary condition to allow fluid flow through that surface (Fig. 1). The superficial (top) and deep (bottom) surfaces of the explant model were frictionless and impermeable. The left most edge of the model (axis of the cylindrical explant) was only constrained in the vertical direction and was also impermeable.

## 2.2. Cell model

The cell and its surroundings were modeled using a sub-modeling function. Following the explant compression simulation which was specified as the 'global' model, the cell model utilized output from the explant model to extract boundary conditions. At each increment the cell model would interpolate the values of the pore pressure and displacement at locations corresponding to the position of its boundary in the explant model and then update its boundary conditions to match these values. The material properties of the ECM were those used for the explant model. The material properties of the PCM, cell and membrane were taken from the literature (Table 2). Cell membranes are much thinner (~5 nm [35]) than the membrane

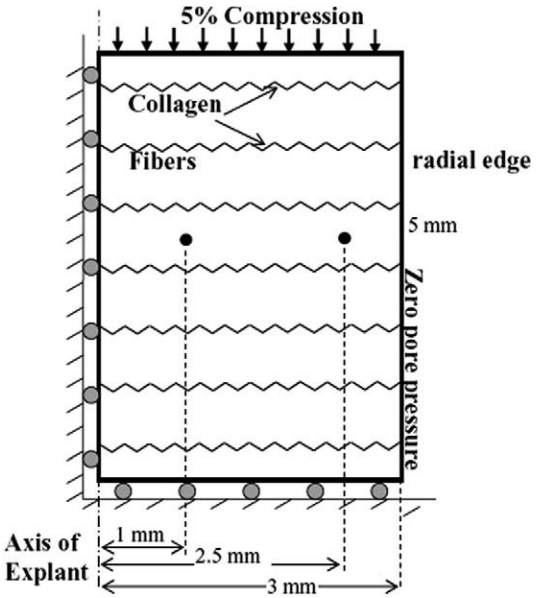


Fig. 1. Schematic of meniscal explant FE model. The collagen reinforcing fibers can be seen, as can the dimensions and boundary conditions of the model. The circular outer cell was located at 2.5 mm from the axis, and the inner cell at 1 mm from the axis. The elliptical cell and small circular cell were only studied at the outer location.

Table 2
Material properties used in the cell model

| Property | ECM (identical to explant model) | PCM [17,42,48] | Membrane [36,42] | Cell [49] |
|---|---|---|---|---|
| Poisson's ratio | 0 | 0.044 | 0.044 | 0.069 |
| Modulus of elasticity MPa (compression) | 0.4 | 0.0665 | 0.0665 | 0.00255 |
| Permeability ($m^4$/N s) | $1.5 \times 10^{-15}$ | $2 \times 10^{-15}$ | $2.5 \times 10^{-20}$ | $2.57 \times 10^{-12}$ |

These material properties belong to chondrons extracted from cartilage.

used in this model (500 nm). Ateshian et al. presented a membrane permeability ($L_p = 5.00 \times 10^{-14}$ $m^3$/N s), that can be multiplied by the thickness of a membrane to determine permeability [36]. This was utilized to determine a permeability for the cell membrane such that it accurately represented the true 5 nm cell membrane.

Quadratic, 2D, poroelastic, continuum elements were used to simulate a homogenous, isotropic ECM, PCM, membrane and cell. Eight-noded continuum plane strain elements with pore pressure active at corner nodes were used (CPE8P). Collagen fibers do not pass through cells or the PCM; therefore, spring elements (SPRINGA) connected the left most edge of the cell model to the right most edge and did not link to any other nodes to simulate the tension compression non-linearity. The term 'left most edge' refers to the periphery of the cell model that is closest to the simulated central axis of the explant in the global model. Similarly, the term 'right most edge' refers to the periphery of the cell model that is closest to the free edge

of the explant model. Again, a coupled pore fluid diffusion and stress analysis was used to analyze the fluid flow velocities, stresses and strains in and around the cell. The position of the cell was specified at two locations within the explant (Fig. 1). Initially a circular cell, placed at a position near the peripheral free edge, 2.5 mm from the central axis of the cylindrical explant (referred to as 'circular outer' due to the shape and location of the cell) was simulated. An identical cell was then placed at a more internal position within the meniscal explant, 1 mm from the central axis (circular inner). The vertical position of the cell within the explant was not altered because the fluid velocity, stress and strain profiles only changed in the radial direction due to the homogeneity of the model. The height of the cell was held at 2.5 mm from the bottom surface. In addition to the location of the cell within the explant, the morphology of the cell was also altered to study the effects this may have on the cellular mechanical environment. While the exact size and shape of the meniscal cells has not previously been quantified, based on chondrocyte studies and our own unpublished observations, a circular cell of 10 μm diameter was studied [17]. The original circular cell of 10 μm diameter was compared to an elliptical cell with a 12.2 μm major axis lying horizontally and an 8.1 μm minor axis lying vertically. The area of the elliptical cell was the same as the area of the circular cell, and was placed at the same 'outer' location as the circular cell. Finally, a circular cell with a diameter of 4.2 μm was studied (small circular) at the same 'outer' location.

In all simulations, the cell was surrounded by a 2.5 μm thick PCM, which included a 0.5 μm thick layer of elements as the cell membrane. Because the purpose of the membrane was to measure the effect of its permeability on the fluid flow shear stress, material properties similar to those of the PCM were used and the permeability was set to $2.5 \times 10^{-20}$ m$^4$/N s [36] (Table 2). Since the cell volume fraction for meniscal tissue is unknown, experimental data for articular cartilage was used to get a cell volume fraction of 7.5% [37,38]. The chondron was encompassed by the ECM which filled a square area 50 μm × 50 μm around the cell (Fig. 2). The ECM elements of the submodel were 1 μm × 1 μm and even smaller in the PCM and cell.

### 2.3. Data analysis

The magnitude of FFISS around the periphery of the cell was calculated using commercially available software (MATLAB, The MathWorks Inc., Natick, MA) and the fluid velocity gradient. Although the cell was permeable, fluid primarily moved over the surface of the cell membrane due to the membrane's low permeability. Using MATLAB, the shear stress on the surface of the cell at each node was then calculated as:

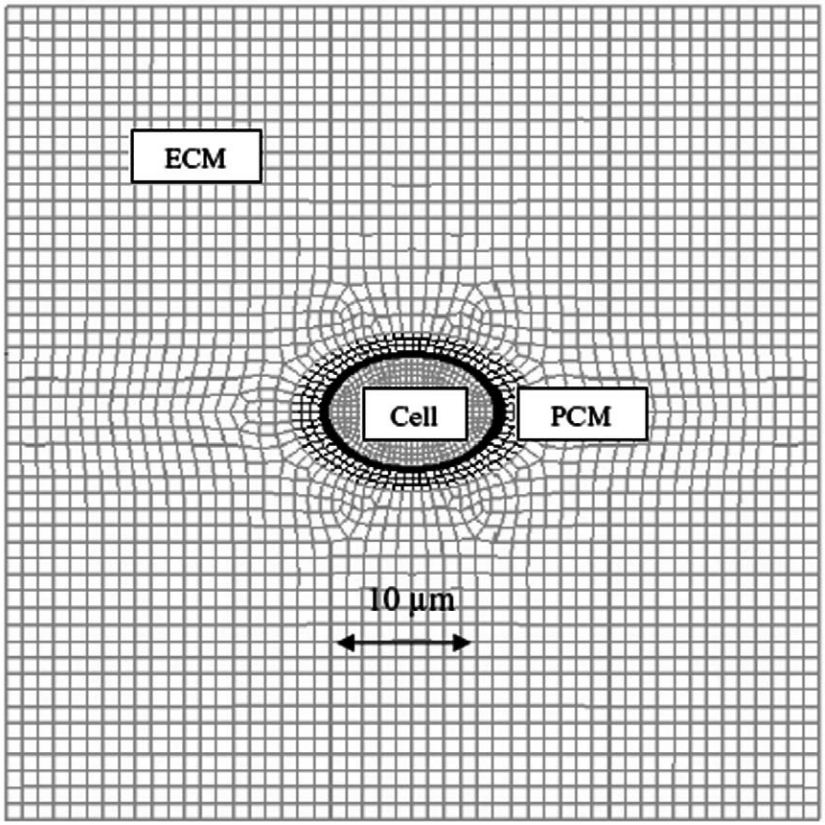


Fig. 2. Elliptical cell submodel showing the cell, PCM and ECM. The membrane lies at the cell–PCM interface and is shown as a blacked region. Length and height of this model is 50 μm. The circular model simply has a circular cell morphology instead of elliptical.

Table 3
Dependence of maximum fluid velocity, pore pressure, principal logarithmic strain and principal stress on elastic modulus, collagen stiffness, permeability and Poisson's ratio

| | Maximum fluid velocity (μm/s) | Maximum pore pressure (MPa) | Principal logarithmic strain (%) | Principal stress (MPa) |
|---|---|---|---|---|
| Elastic modulus (0.3–0.6 MPa) | 25–27.5 | 8.2–8.3 | 5.1–5.3 | 0.02–0.03 |
| Collagen stiffness (50–200 N/mm) | 14.2–32 | 2.8–11.1 | 5.1 | 0.02 |
| Permeability ($0.6–1.5\times10^{-15}$ $m^4$/N s) | 17–27.5 | 8.3 | 5.1 | 0.02 |
| Poisson's ratio (0–0.4) | 27.5 | 8.3 | 5.1 | 0.02 |

As the collagen stiffness or permeability increases, the maximum fluid velocities increase linearly (with the maximum value at the free surface of the explant). An increase in the elastic modulus of the matrix resulted in a drop in maximum fluid velocities. Increases in collagen stiffness increased pore pressure. Minimal changes in maximum pore pressure, strain or stress were found in the ECM with changes in Poisson's ratio or permeability.

$$\mathbf{v} = \mathbf{R}\mathbf{v}^*$$

$$\tau = \frac{v_t^{(2)} - v_t^{(1)}}{dn}$$

where $dn$ is the distance from node (1) on the surface of the cell to node (2) which is perpendicular to the tangent at node (1), $v_t^{(1)}$ is the velocity component at node (1) tangential to the surface of the cell, $v_t^{(2)}$ is the velocity component at node (2) parallel to $v_t^{(1)}$, $\tau$ is the fluid flow induced shear stress at the cell surface, $\mathbf{v}^*$ is the velocity vector expressed in global coordinates, $\mathbf{v}$ is the velocity vector expressed in local coordinates, normal and tangential to the surface of the cell, $\mathbf{R}$ is the rotation matrix that transforms the global velocity vector into the local velocity vector with components tangential and normal to each node on the surface of the cell.

## 3. Results

### 3.1. Explant model

Under 5% unconfined compression, fluid pressure decreased from 8.33 MPa at the central axis of the explant to zero at the peripheral edge and fluid velocities increased from zero at the central axis to their maximum value at the periphery (~27.5 μm/s). There was no change in fluid pressure or fluid velocity through the depth of the material. Changes in elastic modulus, collagen stiffness, and permeability of the ECM had the greatest effects on maximum fluid velocity in the explant model (Table 3). Maximum principal stresses and strains occurred in the radial direction in the explant model. Maximum pore pressure, maximum principal logarithmic strains and maximum principal stresses were not dependent on permeability or Poisson's ratio over the range studied using this model, and collagen stiffness only affected fluid velocities and pore pressure (Table 3). Maximum fluid velocities were increased with increases in permeability, collagen stiffness and strain rate while increases in the elastic modulus decreased the maximum fluid velocities. For all conditions studied, the principal stress and principal strain generally followed a profile similar to that of pore pressure, that is, decreasing from a maximum value at the axis to zero at the peripheral free edge of the explant, and fluid velocities followed a profile inversely proportional to the rate of change of pore pressure along the radius as expected from Darcy's law.

### 3.2. Cell (submodel analysis)

Since both compressive and tensile principal stresses and strains were seen around cells, data was expressed as ranges in the cell, PCM or ECM. Cellular stresses were an order of magnitude less than PCM stresses and were greater in compression for cells in the outer position, near the free edge of

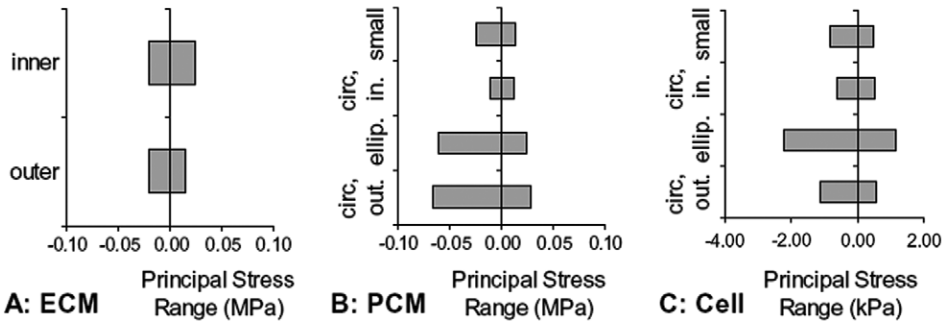


Fig. 3. (A) Range of principal stresses in the absence of the cell within the inner and outer regions of the ECM; (B) range of principal stresses in the PCMs of the four submodels; (C) range of principal stresses within the cells themselves. The lower limits of these ranges represent the largest compressive stresses (negative) and the upper limits represent the largest tensile (positive) stresses. Circ. out. (circular cell at 2.5 mm from axis of explant), ellip (elliptical cell at 2.5 mm from axis of explant), circ. in. (circular cell at 1 mm from axis of explant), and small (circular cell of 4.2 μm diameter at 2.5 mm from axis of explant).

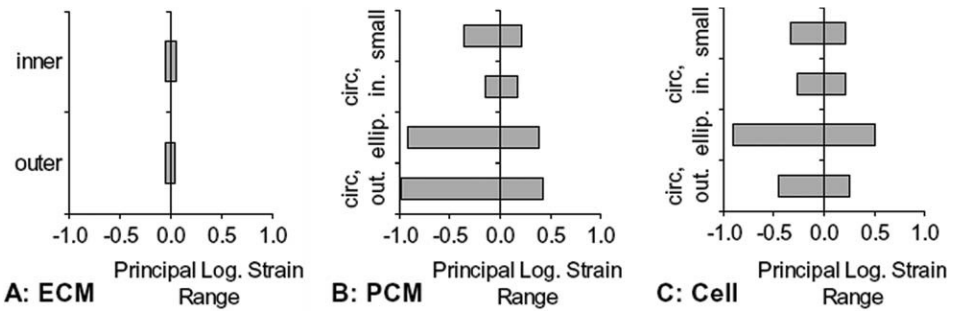


Fig. 4. (A) Range of principal logarithmic strains in the absence of the cell within the inner and outer regions of the ECM; (B) range of principal logarithmic strains in the PCMs of the four submodels; (C) range of principal logarithmic strains within the cells themselves. The lower limits of these ranges represent the largest compressive logarithmic strains (negative) and the upper limits represent the largest tensile (positive) logarithmic strains. Circ. out. (circular cell at 2.5 mm from axis of explant), ellip (elliptical cell at 2.5 mm from axis of explant), circ. in. (circular cell at 1 mm from axis of explant), and small (circular cell of 4.2 μm diameter at 2.5 mm from axis of explant).

the explant (Fig. 3C). The elliptical cell was exposed to a stress range twice that of a circular cell in the same location of the same volume (elliptical versus circular outer) (Fig. 3C). Thus, the PCM of the elliptical cell was less effective at shielding the cell from large stresses, despite similar principal stresses in the PCM of both the circular and elliptical cell of the same volume. The smaller volume circular cell and the circular cell placed closer to the central axis of the explant developed principal stresses similar to the larger volume circular outer cell despite differences in PCM stresses.

Chondrons experienced higher strains than the surrounding ECM (Fig. 4). Strains were greater in the elliptical cell by 98% and were reduced in the inner circular cell by 32% when compared to the circular outer cell. Interestingly, while the stresses in the cell were much smaller than the PCM, the strains within the cells were similar to strains in their PCMs. The PCM of the inner circular cell experienced a range of strains 77% less than the outer circular cell (Fig. 4B). Large compressive strains were produced in small areas of the PCM (Fig. 4B) at a location closest to the cell surface at an angular position of 0° (Fig. 5). Table 4 shows the change in height and length of each cell following compression. While the smaller cell deformed more uniformly, having comparable changes in both height (−16%) and length (+19%), larger cells of both elliptical and circu-

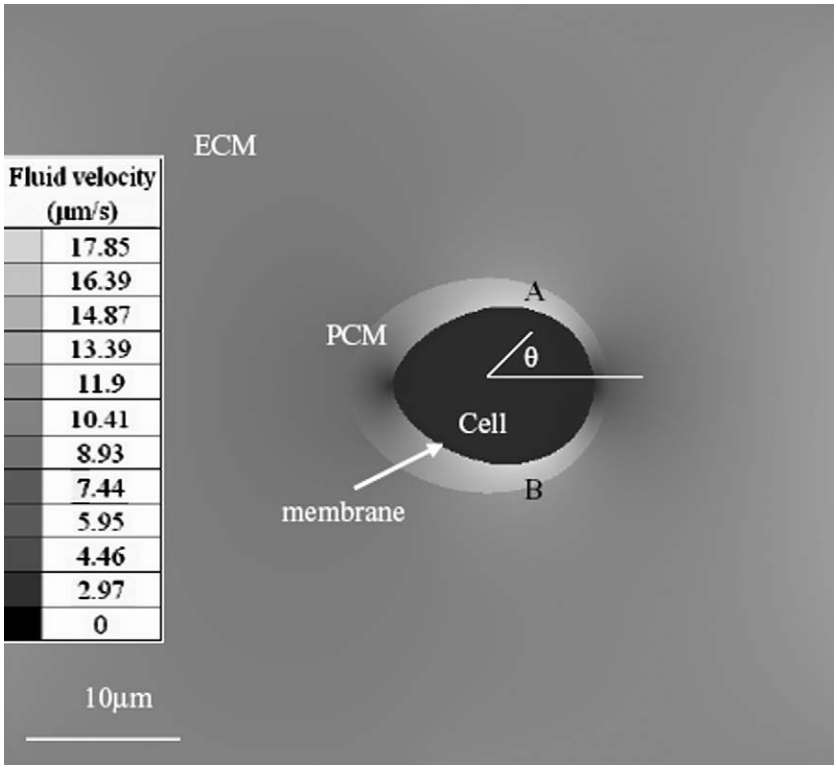


Fig. 5. Contour plot of fluid velocity (μm/s) around the circular cell in a matrix deformed 5% at the global level. The high fluid velocities at 'A' and 'B' around the cell are basically contained within the PCM. A deformed circular cell is shown at 2.5 mm from the axis.

Table 4
Volume, height and length changes for the cells modeled: the circular cell at the two locations, outer and inner, the elliptical cell and the small cell at the outer location immediately following 5% unconfined compression over 1 s

| | Volume (%) | Height (%) | Length (%) |
|---|---|---|---|
| Circular outer | 20 | −8 | 25 |
| Elliptical outer | 15 | 3 | 24 |
| Circular inner | 17 | −2 | 33 |
| Small circular | 21 | −16 | 19 |

lar morphology and at both inner and outer locations, experienced greater increases in length (24–33%) than changes in height (−8% to +3%).

The greater permeability of the PCM compared to the ECM resulted in the largest fluid velocities being generated immediately around the cell, within the PCM (Fig. 5). Fluid velocities were negligible within the cell due to the relatively low permeability of the membrane surrounding it. The maximum magnitude of fluid velocities around an elliptical cell was 21% lower than those around the circular cell at the same location within the explant (Fig. 6A). The inner circular cell experienced maximum fluid velocities only 4% of those around the outer circular cell (Fig. 6B). Decreasing the volume of the circular cell from 78.5 $\mu m^2$ (diameter 10 μm) to 13.8 $\mu m^2$ (diameter 4.2 μm) increased fluid velocities in the PCM.

Fluid flow induced shear stress followed a similar profile to that of fluid velocity. Fluid flow induced shear stresses were zero for all cases at an angular position of 0° and 180° on the surface of the cell (Fig. 5). As fluid velocities increased at points A and B on the cell, so did the fluid flow induced shear stresses (Fig. 7).

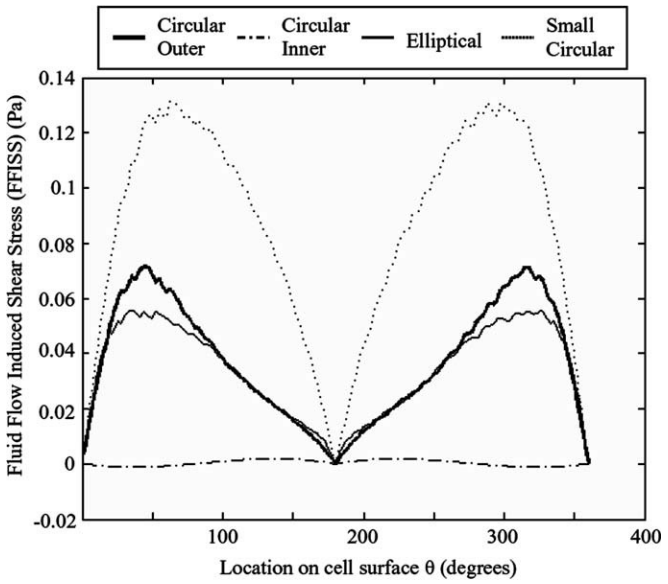


Fig. 7. Fluid flow shear stress (Pa) vs. angle around cell measured in degrees from the positive horizontal axis (a horizontal line running through the center of the cell as shown in Fig. 5).

## 4. Discussion

The findings of this study expand on the previous knowledge of the mechanical environment in biphasic tissues, and in particular the mechanical environment around an individual cell [13,15,17–19,39–41]. The data presented are novel, in that a range of tissue properties for meniscal tissue was investigated to study the effects on the mechanical environment within a meniscal explant. Changes in the meniscal material properties tended to have the largest effects on interstitial fluid velocities, more than doubling the value (from 14 to 32 μm/s). Thus, these data agree with previous results that cells within different regions of the explant will be exposed to different magnitudes of mechanical stimuli depending on their position within the tissue and the mechanical properties of the tissue surrounding them [14,18]. How the mechanical environment changes with altered material properties may also be of value when considering trauma, or degeneration that may likely cause meniscal tissue to remodel with new material properties. While the material properties of degenerative meniscal tissue are unknown, and the current results only examined a range, it may be extrapolated that if large changes in the elastic modulus occur with degeneration, or changes in permeability, then fluid flow characteristics and solid matrix behavior will be dramatically affected.

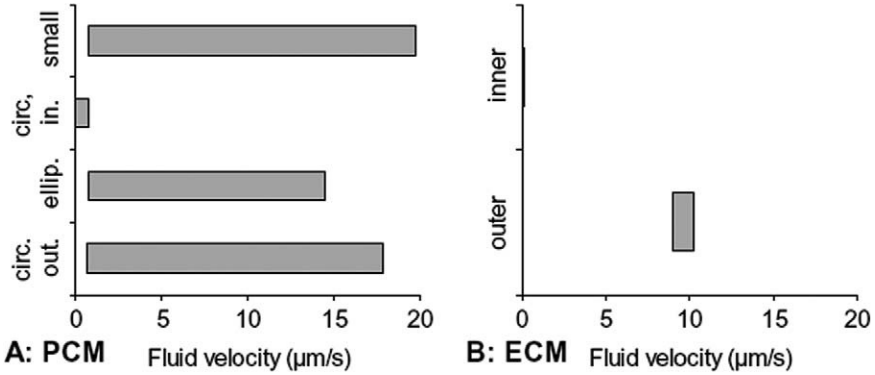


Fig. 6. (A) Range of fluid velocities seen in the submodels. (B) Range of magnitudes of fluid velocity in the absence of the cell at 1 mm from the axis (inner) and at 2.5 mm from the axis (outer). Circ. out. (circular cell at 2.5 mm from axis of explant), ellip (elliptical cell at 2.5 mm from axis of explant), circ. in. (circular cell at 1 mm from axis of explant), and small (circular cell of 4.2 μm diameter at 2.5 mm from axis of explant).

This research is the first to study the cellular mechanical environment in which the cell was modeled with a semi-permeable membrane, and the gradient of the fluid velocity was used to calculate an estimated FFISS. This study provides greater insight into the effect of varying shape and position of chondrons which appear to be stress and strain concentrators within meniscal tissue. While it has previously been shown that cells are shielded from high stresses by their PCMs [17], the higher permeability of the PCM coupled with a membrane with a low permeability results in higher fluid velocities tangential to the cell surface and thus high fluid flow induced shear stress. Principal strains within cells remained comparable to strains in the PCM regardless of this stress shielding effect. An elliptical cell morphology increases the principal stresses and principal strains within the cell. This may mean that cells in the meniscus, which are elliptical, are more sensitive to their mechanical environments. Cell strain has previously been shown to correlate to matrix synthesis [13]. This model predicts that a cell may increase in volume immediately following compression by approximately 20%, which is in agreement with other such models [18] that did not include a cell membrane. Wu et al. showed that while cell volume increases initially following a ramp compression, cell volumes then decrease as the tissue is allowed to relax [18], which is in agreement with experimental evidence of cell volumes decreasing at equilibrium under a compressive strain [39]. Volume changes in this paper may not be realistic because the membrane did not contain any ruffles or undulations which may affect volume changes [39]. Volume changes cannot be computed from height and length changes alone as the morphology of cells modeled did not remain elliptical or circular following compression.

Chondrons closer to the radial edge will be exposed to higher fluid velocities as shown by the macroscopic fluid velocity profile. However, due to the shielding effect of the PCM there were only small changes in the cellular principal stresses and principal strains with varying cell location, even though the principal stresses and principal strains in the PCM showed large changes with position. Kim and Buschmann [13–15] found that matrix synthesis was greatest at the free surface of the explant and decreased at the center of a cylindrical cartilage explant. Current results showed that the most pronounced manifestation of a change in radial position on a cell was the alteration of fluid velocities tangential to the cell, and thus fluid flow or associated streaming potentials may play an important role in mechanotransduction. The presence of a membrane increased the tangential component of fluid velocity and consequently the fluid flow induced shear stress by an order of magnitude (data not shown). Due to the higher permeability of the cell compared to the ECM and PCM, without the relatively impermeable cell membrane, maximum fluid velocities occurred in the cell itself, as the cell offered less resistance to flow and fluid preferentially flowed through the cell. Another potent influence on fluid velocities is cell size. Smaller cells experience greater fluid flow induced shear stresses even though fluid velocities around them are only slightly greater than velocities around larger cells. Recent studies have shown that the permeability of chondrocyte PCMs may be on the order of $10^{-17}$ $m^4/N$ s [42], which reduces fluid flow around the cell in comparison to this model.

Fluid flow induced shear stresses have previously been shown to result in increases in intracellular calcium concentration in meniscal cells. These studies however were conducted with fluid shear stresses ~1–6 Pa [23,43]. Future studies should be conducted at the smaller shear stress levels seen in this study (<1.0 Pa). Previous studies on articular cartilage have used shear stress levels from 1 Pa to 3.7 Pa [21,22]. These studies did show that at 1 Pa, approximately 40% of the cells responded with an increase in intracellular calcium mobilization [21]. Intracellular calcium is a potent second messenger in many musculoskeletal cells. Fibroblasts have also been shown to be sensitive to fluid flow induced shear stresses with magnitudes between 0.7 Pa and 2.5 Pa [20,44]. We are uncertain if meniscal cells would be responsive to the magnitudes found in this study. Fluid flow in musculoskeletal tissues results in a complex environment around cells, creating a potential mechanical signal, streaming potential and/or chemotransport detectable by the cell. Previous researchers have shown that the degree of matrix synthesis is similar to the fluid velocity profile within cartilage explants [15], and studies in bone have shown that chemotransport can modulate the response of bone cells to fluid flow induced shear stress [45]. Thus, since meniscal tissue is composed of both fibroblastic-like cells and chondrocytic-like cells, future biological studies should separate meniscal cell populations and determine the mechanosensitivity to fluid flow induced shear stress below 1 Pa as predicted by this model.

Early studies on meniscal cell morphology suggested that in the superficial zone of the tissue there exist fibroblastic-like cells, and in the deeper zones there existed more chondrocytic or spherical cells [16,46]. Recently, some have begun to suggest that near the peripheral attachment to the joint capsule there exist more fibroblastic-like cells and in the inner zone, near the central apex, the cells are more chondrocytic-like [12]. Therefore, how cell morphology changes throughout the meniscus is unknown, and needs further 3D studies. Since we modeled the tissue as homogeneous, and there were no changes in ECM stresses through the depth of the tissue, we can assume that we are simply modeling two different cell morphologies. Whether they occur in superficial or deep zones, or inner versus outer zones, will require more studies.

Both models in this study were 2D whereas the true environment is 3D. In reality tensile elements (collagen) are unidirectional and this may result in different loading of the cell in a direction running perpendicular to the collagen fibers. A truly 3D model of an explant would allow for a complete analysis of the mechanical loading on cells. For example, fluid velocities are lower if tension elements are not included in the global explant model by two orders

of magnitude. Hence, the 3D environment around a cell will likely be affected by the non-uniform orientation of collagen fibers in the meniscus.

While constant material properties were assumed for the cell and PCM, previous FE models have studied how these properties affect the local mechanical environment around cells [17,47]. Some have shown that the permeability of the cell relative to that of the extracellular matrix does not have a large influence on the mechanical environment [17], whereas more recently, decreases in Young's modulus and increases in permeability of the PCM, changes associated with osteoarthritis, resulted in increases in cell compressive strain [47]. It should be noted, however, that these previous FE models were of articular cartilage and used a linear biphasic model. Future work should include determining the range of material properties for meniscal cells isolated from various regions of the tissue as well as incorporating ECM inhomogeneities that may exist. This could then provide a basis for a parametric study of the affect of material properties of the cell and PCM in meniscal tissue.

## 5. Conclusion

The mechanical environment of chondrons is governed in part by their position relative to a free edge, material properties of the constituents of the cell, PCM, membrane and ECM, as well as their morphology and size. In particular cells are shielded from high stresses by the PCM whereas cellular strains are comparable to strains in the PCM. Chondrons act as stress and strain concentrators. Elliptical cells are more sensitive to external loading with the exception of fluid flow induced shear stress which is higher in circular cells. A cell membrane was found to be crucial in magnifying the tangential fluid flow and hence the induced shear stress around a cell. Furthermore, the smaller a cell the greater the fluid velocity shear stresses around it. The role of fluid flow needs to be studied in more detail as FFISS were lower than those which caused a cellular response in previous studies. Disease states such as osteoarthritis affect the material properties of the ECM and, as shown in this study, the mechanical environment within an explant changes appreciably with changes in material properties.

## Acknowledgements

We would like to thank the Whitaker Foundation for their financial support under grant #RG-03-0047, Dr. Jeff Allen for consultation on fluid shear stresses, and Dr. Gerard Ateshian for his consultation on membrane permeabilities.

## References

[1] Anderst WJ, Tashman S. A method to estimate in vivo dynamic articular surface interaction. J Biomech 2003;36(9):1291–9.

[2] Ahmed AM, Burke DL. In-vitro measurement of static pressure distribution in synovial joints – Part I: Tibial surface of the knee. J Biomech Eng 1983;105(3):216–25.

[3] Voloshin AS, Wosk J. Shock absorption of meniscectomized and painful knees: a comparative in vivo study. J Biomed Eng 1983;5(2):157–61.

[4] Haut Donahue TL, Hull ML, Rashid MM, Jacobs CR. The sensitivity of tibiofemoral contact pressure to the size and shape of the lateral and medial menisci. J Orthop Res 2004;22(4):807–14.

[5] Englund M, Lohmander LS. Risk factors for symptomatic knee osteoarthritis fifteen to twenty-two years after meniscectomy. Arthritis Rheum 2004;50(9):2811–9.

[6] Cicuttini FM, Forbes A, Yuanyuan W, Rush G, Stuckey SL. Rate of knee cartilage loss after partial meniscectomy. J Rheumatol 2002;29(9):1954–6.

[7] Zielinska B, Donahue TL. 3D finite element model of meniscectomy: changes in joint contact behavior. J Biomech Eng 2006;128(1):115–23.

[8] Adams ME, Hukins DWL. The extracellular matrix. In: Mow VC, Arnoczky SP, Jackson DW, editors. Knee meniscus: basic and clinical foundations. New York, NY: Raven Press; 1994.

[9] Mow VC, Ratcliffe A, Chern KY, Kelly MA. Structure and function relationships of the menisci of the knee. In: Mow VC, Arnoczky SP, Jackson DW, editors. Knee meniscus: basic and clinical foundations. New York, NY: Raven Press; 1994.

[10] Djurasovic M, Aldridge JW, Grumbles R, Rosenwasser MP, Howell D, Ratcliffe A. Knee joint immobilization decreases aggrecan gene expression in the meniscus. Am J Sports Med 1998;26(3):460–6.

[11] Vailas AC, Zernicke RF, Matsuda J, Curwin S, Durivage J. Adaptation of rat knee meniscus to prolonged exercise. J Appl Physiol 1986;60(3):1031–4.

[12] Upton ML, Chen J, Guilak F, Setton LA. Differential effects of static and dynamic compression on meniscal cell gene expression. J Orthop Res 2003;21(6):963–9.

[13] Kim YJ, Sah RL, Grodzinsky AJ, Plaas AH, Sandy JD. Mechanical regulation of cartilage biosynthetic behavior: physical stimuli. Arch Biochem Biophys 1994;311(1):1–12.

[14] Buschmann MD, Kim YJ, Wong M, Frank E, Hunziker EB, Grodzinsky AJ. Stimulation of aggrecan synthesis in cartilage explants by cyclic loading is localized to regions of high interstitial fluid flow. Arch Biochem Biophys 1999;366(1):1–7.

[15] Kim YJ, Bonassar LJ, Grodzinsky AJ. The role of cartilage streaming potential, fluid flow and pressure in the stimulation of chondrocyte biosynthesis during dynamic compression. J Biomech 1995;28(9):1055–66.

[16] Hellio Le Graverand MP et al. The cells of the rabbit meniscus: their arrangement, interrelationship, morphological variations and cytoarchitecture. J Anat 2001;198(Pt 5):525–35.

[17] Guilak F, Mow VC. The mechanical environment of the chondrocyte: a biphasic finite element model of cell–matrix interactions in articular cartilage. J Biomech 2000;33(12):1663–73.

[18] Wu JZ, Herzog W. Finite element simulation of location- and time-dependent mechanical behavior of chondrocytes in unconfined compression tests. Ann Biomed Eng 2000;28(3):318–30.

[19] Baer AE, Setton LA. The micromechanical environment of intervertebral disc cells: effect of matrix anisotropy and cell geometry predicted by a linear model. J Biomech Eng 2000;122(3):245–51.

[20] Hung CT, Allen FD, Pollack SR, Attia ET, Hannafin JA, Torzilli PA. Intracellular calcium response of ACL and MCL ligament fibroblasts to fluid-induced shear stress. Cell Signal 1997;9(8):587–94.

[21] Yellowley CE, Jacobs CR, Li Z, Zhou Z, Donahue HJ. Effects of fluid flow on intracellular calcium in bovine articular chondrocytes. Am J Physiol 1997;273(1 Pt 1):C30–6.

[22] Yellowley CE, Jacobs CR, Donahue HJ. Mechanisms contributing to fluid-flow-induced $Ca^{2+}$ mobilization in articular chondrocytes. J Cell Physiol 1999;180(3):402–8.

[23] Eifler RL, Blough ER, Dehlin JM, Haut Donahue TL. Oscillatory fluid flow regulates glycosaminoglycan production via an intracellular calcium pathway in meniscal cells. J Orthop Res 2006;24(3):375–84.

[24] Spilker RL, Donzelli PS, Mow VC. A transversely isotropic biphasic finite element model of the meniscus. J Biomech 1992;25(9):1027–45.
[25] Krishnan R, Park S, Eckstein F, Ateshian GA. Inhomogeneous cartilage properties enhance superficial interstitial fluid support and frictional properties, but do not provide a homogeneous state of stress. J Biomech Eng 2003;125(5):569–77.
[26] Mow VC, Kuei SC, Lai WM, Armstrong CG. Biphasic creep and stress relaxation of articular cartilage in compression? Theory and experiments. J Biomech Eng 1980;102(1):73–84.
[27] Soulhat J, Buschmann MD, Shirazi-Adl A. A fibril-network-reinforced biphasic model of cartilage in unconfined compression. J Biomech Eng 1999;121(3):340–7.
[28] Huang CY, Soltz MA, Kopacz M, Mow VC, Ateshian GA. Experimental verification of the roles of intrinsic matrix viscoelasticity and tension–compression nonlinearity in the biphasic response of cartilage. J Biomech Eng 2003;125(1):84–93.
[29] Tissakht M, Ahmed AM. Tensile stress–strain characteristics of the human meniscal material. J Biomech 1995;28(4):411–22.
[30] Hunter SA, Noyes FR, Haridas B, Levy MS, Butler DL. Effects of matrix stabilization when using glutaraldehyde on the material properties of porcine meniscus. J Biomed Mater Res 2003;67(4):1245–54.
[31] Proctor CS, Schmidt MB, Whipple RR, Kelly MA, Mow VC. Material properties of the normal medial bovine meniscus. J Orthop Res 1989;7(6):771–82.
[32] Favenesi JA, Shaffer JC, Mow VC. Biphasic mechanical properties of knee mensicus. In: 29th Annual Meeting, Orthopaedic Research Society, Anaheim, CA, 1983.
[33] LeRoux MA, Ateshian GA, Parker T, Setton LA. Effects of colleagen fiber anisotropy on the hydraulic permeability of the meniscus. In: 47th annual meeting, Orthopaedic Research Society, San Francisco, CA, 2001.
[34] Fithian DC, Zhu WB, Ratcliffe A, Kelly MA, Mow VC, Malinin TI. Exponential law representation of tensile properties of human meniscus. Proc Inst Mech Eng Bioeng 1989;203:85–90.
[35] Alberts B, Bray D, Lewis J, Raff M, Roberts K, Watson JD. Molecular biology of the cell. 3rd ed. New York, NY: Garland; 1994.
[36] Ateshian GA, Likhitpanichkul M, Hung CT. A mixture theory analysis for passive transport in osmotic loading of cells. J Biomech 2006;39(3):464–75.
[37] Wong M, Wuethrich P, Buschmann MD, Eggli P, Hunziker E. Chondrocyte biosynthesis correlates with local tissue strain in statically compressed adult articular cartilage. J Orthop Res 1997;15(2):189–96.
[38] Stockwell RA. Chondrocytes. J Clin Pathol Suppl (R Coll Pathol) 1978;12:7–13.
[39] Guilak F. Compression-induced changes in the shape and volume of the chondrocyte nucleus. J Biomech 1995;28(12):1529–41.
[40] Bachrach NM, Valhmu WB, Stazzone E, Ratcliffe A, Lai WM, Mow VC. Changes in proteoglycan synthesis of chondrocytes in articular cartilage are associated with the time-dependent changes in their mechanical environment. J Biomech 1995;28(12):1561–9.
[41] Wilson W, van Donkelaar CC, van Rietbergen B, Ito K, Huiskes R. Stresses in the local collagen network of articular cartilage: a poroviscoelastic fibril-reinforced finite element study. J Biomech 2004;37(3):357–66.
[42] Alexopoulos LG, Williams GM, Upton ML, Setton LA, Guilak F. Osteoarthritic changes in the biphasic mechanical properties of the chondrocyte pericellular matrix in articular cartilage. J Biomech 2005;38(3):509–17.
[43] Mroz JM, Donahue SW, Haut Donahue TL. Increases in intracellular calcium due to oscillating fluid flow are shear stress dependent in meniscal cells. In: 49th annual meeting, Orthopaedic Research Society, New Orleans, LA, 2003.
[44] van der Pauw MT, Klein-Nulend J, van den Bos T, Burger EH, Everts V, Beertsen W. Response of periodontal ligament fibroblasts and gingival fibroblasts to pulsating fluid flow: nitric oxide and prostaglandin E2 release and expression of tissue non-specific alkaline phosphatase activity. J Periodont Res 2000;35(6):335–43.
[45] Donahue TL, Haut TR, Yellowley CE, Donahue HJ, Jacobs CR. Mechanosensitivity of bone cells to oscillating fluid flow induced shear stress may be modulated by chemotransport. J Biomech 2003;36(9):1363–71.
[46] Nakata K et al. Human meniscus cell: characterization of the primary culture and use for tissue engineering. Clin Orthop 2001(391 Suppl):S208–18.
[47] Alexopoulos LG, Setton LA, Guilak F. The biomechanical role of the chondrocyte pericellular matrix in articular cartilage. Acta Biomater 2005;1:317–25.
[48] Alexopoulos LG, Haider MA, Vail TP, Guilak F. Alterations in the mechanical properties of the human chondrocyte pericellular matrix with osteoarthritis. J Biomech Eng 2003;125(3):323–33.
[49] Leipzig ND, Athanasiou KA. Unconfined creep compression of chondrocytes. J Biomech 2005;38(1):77–85.